

# Optical conductivity of layered topological semimetal TaNiTe<sub>5</sub>

Jakov Budić,<sup>1,\*</sup> Serena Nasrallah,<sup>2,\*</sup> D. Santos-Cottin,<sup>3</sup> A. Pulkkinen,<sup>4</sup> J. Minár,<sup>4</sup> P. Sačer,<sup>1</sup> B. Gudac,<sup>1</sup> V. Despoja,<sup>5</sup> N. Barišić,<sup>1,2</sup> C. C. Homes,<sup>6</sup> Ana Akrap,<sup>1,†</sup> and Mario Novak<sup>1,‡</sup>

<sup>1</sup>Department of Physics, Faculty of Science, University of Zagreb, 10000 Zagreb, Croatia

<sup>2</sup>Institute of Solid State Physics, TU Wien, 1040 Vienna, Austria

<sup>3</sup>Department of Physics, University of Fribourg, 1700 Fribourg, Switzerland

<sup>4</sup>New Technologies Research Centre, University of West Bohemia, 30100 Pilsen, Czech Republic

<sup>5</sup>Institute of Physics, 10000 Zagreb, Croatia

<sup>6</sup>National Synchrotron Light Source II, Brookhaven National Laboratory, Upton, New York 11973, USA

(Dated: November 17, 2025)

We present an infrared spectroscopy study of the layered topological semimetal TaNiTe<sub>5</sub>, a material with a quasi-one-dimensional structure and strong in-plane anisotropy. Despite its structural features, infrared reflectivity and electronic transport measurements along the *a* and *c* crystallographic axes show metallic behavior without evidence of reduced dimensionality. Optical conductivity reveals an anisotropic but conventional metallic response with low scattering rates and a single sharp infrared-active phonon mode at 396 cm<sup>-1</sup> (49 meV). *Ab initio* calculations closely match the experimental optical data and confirm a three-dimensional electronic structure. Our results demonstrate that TaNiTe<sub>5</sub> behaves as a three-dimensional anisotropic semimetal in its electronic and optical properties.

## I. INTRODUCTION

Many emerging technologies increasingly rely on the unique electronic properties of van der Waals telluride materials [1, 2]. TaNiTe<sub>5</sub> is a topological semimetal characterized by a chain-like atomic structure and strong in-plane electronic anisotropy. This material was reported to host a variety of complex electronic structures, including quasi-one-dimensionality, Dirac nodal lines, nodal loops, and fourfold Dirac cones protected by non-symmorphic symmetry, which remain stable in the presence of spin-orbit coupling [3–6]. TaNiTe<sub>5</sub> also shows high magnetoresistance and low effective carrier masses [7]. Further studies have indicated that TaNiTe<sub>5</sub> may exhibit a three-dimensional topological character, supported by quantum oscillations [8] and scanning tunneling microscopy measurements [9]. This raises questions about the actual dimensionality of its electronic structure. To investigate this, we determined the complex optical conductivity, which can reveal features of low-dimensional systems, such as van Hove singularities.

In this work, we have determined the infrared reflectivity and electronic transport along the *a* and *c* crystallographic axes. Reflectivity spectra indicate metallic behavior in both directions. Resistivity data show anisotropy and a linear temperature dependence above 100 K, consistent with a dominant role of electron-phonon scattering. No spectral features indicative of reduced dimensionality were observed. The experimental optical response agrees well with *ab initio* calculations.

Our results show that TaNiTe<sub>5</sub> is an anisotropic semimetal without clear signatures of low-dimensional

electronic behavior. The agreement between experiment and *ab initio* calculations further supports a three-dimensional electronic structure, despite the quasi-one-dimensional-like material structure.

## II. EXPERIMENTAL DETAILS

Single crystals of TaNiTe<sub>5</sub> have been synthesized using a self-flux method, with the ratio Ta : Ni : Te = 1 : 1 : 10. High-purity elements have been sealed in a quartz tube under a vacuum of 10<sup>-5</sup> mbar and heated to 950 °C, below the boiling point of tellurium, to dissolve and homogenize the flux. Crystallization was carried out by slow cooling, at a rate of 1 K min<sup>-1</sup>, down to 500 °C. Single crystals were then extracted by centrifuge. As a result, shiny, easy-to- cleave crystals are obtained with lateral dimensions (*a*-*c* plane) of about 5 mm × 2 mm. The crystals were characterized by powder X-ray diffraction (PXRD), energy-dispersive X-ray spectroscopy (EDX), and Laue diffraction to confirm their crystal structure, composition, and orientation, respectively.

Resistivity and Hall effect were measured using a home-built setup using the four-contact method. Infrared reflectance was measured using a Bruker Vertex 70v and 80v Fourier transform spectrometers. The reflectivity measurement is performed at a near-normal angle of incidence. Temperature control was achieved using a continuous-flow cryostat with a cold finger. In order to measure the absolute reflectance, an *in situ* gold evaporation technique was used [10]. After the spectra of the sample were measured, a tungsten wire coil was used to evaporate a small amount of gold onto the sample. The measurements were then repeated on the now gold-coated sample. This method allows us to have an almost perfect reference because it takes into account the shape, surface irregularities, and position of the sample.

\* These authors contributed equally

† [aakrap.phy@pmf.hr](mailto:aakrap.phy@pmf.hr)

‡ [mnovak.phy@pmf.hr](mailto:mnovak.phy@pmf.hr)

The reflectivity is a combination of the real and imaginary parts of the dielectric function, and as such can be difficult to interpret. The real part of the optical conductivity, calculated from the imaginary part of the dielectric function, is a more intuitive quantity. Accordingly, the complex dielectric function,  $\tilde{\epsilon}(\omega) = \epsilon_1 + i\epsilon_2$ , has been determined from a Kramers-Kronig analysis of the reflectivity, which requires extrapolations at high and low frequencies. At low frequency a metallic Hagen-Rubens extrapolation,  $R(\omega) = 1 - A\sqrt{\omega}$  was employed, where  $A$  is chosen to match the value of the reflectance at the lowest measured frequency. At high frequency, the reflectivity measurements were extended using ellipsometry results up to 5 eV. At energies above that, the reflectivity can be extrapolated from X-ray scattering functions (XRO) [11, 12]. The complex conductivity,  $\tilde{\sigma}(\omega)$ , is calculated from the complex dielectric function,  $\tilde{\sigma}(\omega) = \sigma_1 + i\sigma_2 = -2\pi i\omega[\tilde{\epsilon}(\omega) - \epsilon_\infty]/Z_0$ , where  $\epsilon_\infty$  high-frequency contribution to the real part of the dielectric function, and  $Z_0 \simeq 377 \Omega$  is the impedance of free space.

*Ab initio* electronic structure calculations were performed with the linearized augmented wave method with local orbitals (LAPW+lo) using the Elk software [13]. The basis set cutoff parameter  $R_{\text{MT}}K_{\text{max}}$  was set to 8.0, and the exchange-correlation effects were included at the level of the generalized gradient approximation (GGA) as implemented in the PBE functional [14]. The optical conductivity was calculated using a dense sampling of the Brillouin zone with a  $45 \times 45 \times 21$   $k$ -point mesh. The occupation numbers were smeared using the Fermi-Dirac distribution with a smearing width of 0.2 mHa. Spin-orbit interaction was included in all calculations. The calculated optical conductivities were broadened by convolution with a Lorentzian function with full width at half maximum 50 meV, and the Drude term describing intraband transitions was added after broadening.

### III. RESULTS AND DISCUSSION

The layered TaNiTe<sub>5</sub> material belongs to the class of van der Waals materials, with an easy cleaving  $a-c$  plane perpendicular to the crystallographic  $b$  axis. It crystallizes in an orthorhombic crystal structure Cmcm (No. 63) with lattice parameters  $a = 3.659 \text{ \AA}$ ,  $b = 13.122 \text{ \AA}$ , and  $c = 15.111 \text{ \AA}$  [15]. The structure is shown in the inset of Fig. 1(a). TaNiTe<sub>5</sub> is composed of 1D polymeric chains of nickel and tantalum along the  $a$  direction, bridged by tellurium atoms. Nickel atoms are octahedrally coordinated, and tantalum atoms are in a strongly disordered square-pyramidal coordination with ligand tellurium atoms.

The resistivity of TaNiTe<sub>5</sub> is shown in Fig. 1 (a). It is metallic in character along both the  $a$  and  $c$  directions, with a linear temperature dependence above  $\approx 50 \text{ K}$ , consistent with electron-phonon scattering. We observe a noticeable anisotropy:  $\rho_a/\rho_c \approx 0.08$  at  $1.8 \text{ K}$  and  $\rho_a/\rho_c \approx 0.18$  at  $300 \text{ K}$ . The residual resistivity is much

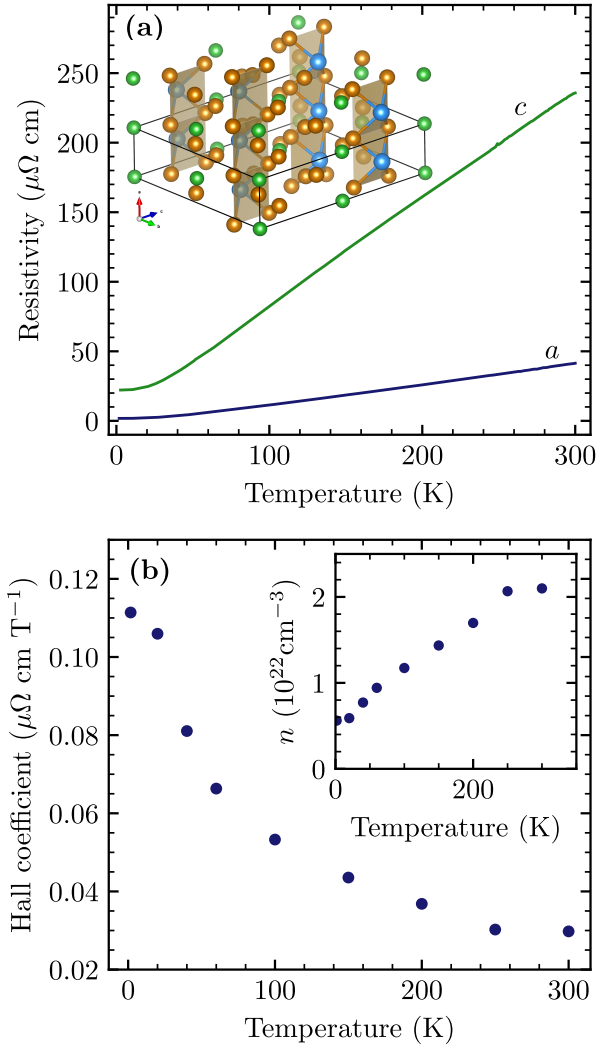


Figure 1. (a) The experimentally-determined temperature dependence of resistivity ( $\rho$ ) for TaNiTe<sub>5</sub> along  $a$  and  $c$  axes. The inset shows TaNiTe<sub>5</sub> structure [16]. (b) Measured temperature dependence of Hall coefficient  $R_H$  for the same sample. The inset shows carrier density at different temperatures calculated using a simple model  $n \propto 1/R_H$ .

larger in the  $c$ -direction, and the temperature dependence is stronger. The Hall coefficient  $R_H$  does not change sign in the measured temperature range, from  $1.8 \text{ K}$  up to  $300 \text{ K}$ . Assuming a single band,  $R_H = 1/ne$ , the number of carriers is of the order of magnitude  $n \approx 10^{22} \text{ cm}^{-3}$ , consistent with the metallic resistivity. The measured  $R_H(T)$  implies that  $n$  decreases at low temperatures, consistent with a semimetallic band structure.

The temperature dependence of the reflectivity measured over a wide frequency range for light polarized along the  $a$  and  $c$  axes is shown in Fig. 2(a) and 2(b), respectively. Despite a large anisotropy in the reflectivity, the response is metallic in both cases, with  $R \rightarrow 1$  in the  $\hbar\omega \rightarrow 0$  limit. The temperature dependence was determined up to  $15\,000 \text{ cm}^{-1}$ , above which it is assumed to have little temperature dependence. The full range,

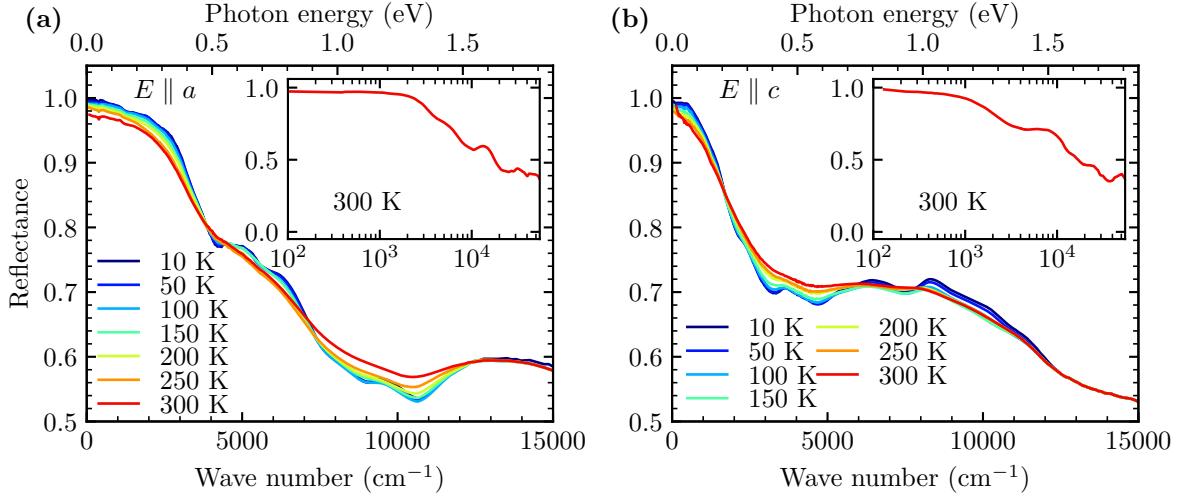


Figure 2. The temperature dependence of the reflectivity of a  $\text{TaNiTe}_5$  single crystal as a function of wave number (photon energy) along the (a)  $a$  axis, and (b)  $c$  axis, up to  $15\,000\,\text{cm}^{-1}$ , above which the temperature dependence is insignificant. The insets show the full range of measured reflectance at room temperature.

up to  $40\,000\,\text{cm}^{-1}$ , at room temperature, is shown in the insets.

To further analyze the optical data, we use Kramers-Kronig transformations to obtain complex optical response functions, specifically the optical conductivity and the dielectric function. The real part of the optical conductivity  $\sigma_1$  at  $10\,\text{K}$  is shown in Figs. 3(a) and 3(c) for light polarized along the  $a$  and  $c$  axis, respectively. The insets show  $\sigma_1$  in a lower energy range on a linear scale. Note that the optical data at energies higher than  $40\,000\,\text{cm}^{-1}$  is extrapolated from X-ray scattering functions (XRO) [11].

To investigate the behavior of the optical properties in more detail, the optical response has been modeled using the Drude-Lorentz model for the complex dielectric function

$$\tilde{\epsilon}(\omega) = \epsilon_\infty - \frac{\omega_p^2}{\omega^2 + i\omega/\tau} + \sum_j \frac{\Omega_j^2}{\omega_j^2 - \omega^2 - i\omega\gamma_j}. \quad (1)$$

In the first term  $\omega_p^2 = 4\pi ne^2/m^*$  and  $1/\tau$  are the square of the plasma frequency and scattering rate for the delocalized (Drude) carriers, respectively, and  $n$  and  $m^*$  are the carrier concentration and effective mass. In the summation,  $\omega_j$ ,  $\gamma_j$  and  $\Omega_j$  are the position, width, and strength of a symmetric Lorentzian oscillator that describe the  $j$ th vibration or bound excitation. The term  $\epsilon_\infty$  is meant to capture the contributions to the real part of the dielectric function from high-frequency excitations.

The infrared reflectance was fitted using a nonlinear least-squares approach, and then the optical conductivity was calculated. In addition to the bound excitations, the anisotropic response of the free carriers is revealed through the plasma frequency and the scattering rate;

$1/\tau$  is shown in the insets of Figs. 3(b) and 3(d) as a function of temperature along the  $a$  and  $c$  axes, respectively. The plasma frequency calculated from the Drude-Lorentz fit is roughly temperature independent and amounts to  $\omega_{p,a} \approx 32\,000\,\text{cm}^{-1}$  in  $a$  direction and  $\omega_{p,c} \approx 21\,000\,\text{cm}^{-1}$  in  $c$  direction. The ability to separate the two Drude parameters,  $1/\tau$  and  $\omega_p$ , is an advantage of optical conductivity. The Drude plasma frequency  $\omega_p$ , and the scattering rate can be related to resistivity,

$$\rho = \frac{4\pi}{\omega_p^2} \frac{1}{\tau}. \quad (2)$$

However, the low-frequency reflectance in  $\text{TaNiTe}_5$  is quite close to unity. Since  $\sigma_1(\omega) \propto 1/[1 - R(\omega)]$ , a small uncertainty in reflectance in this region significantly affects optical conductivity. This yields a relatively high uncertainty for the scattering rate  $1/\tau$ .

The scattering rate  $1/\tau$  at lower temperatures is higher for the  $c$  direction, while the plasma frequency  $\omega_p$  has little to no temperature dependence. The results are therefore consistent with the resistivity data. The temperature dependence of the scattering rate seems to be linear, especially at lower temperatures. Furthermore, the anisotropy can be seen between  $a$  and  $c$  directions; however, it becomes less apparent as the temperature increases.

A single infrared active phonon can be seen at  $\approx 396\,\text{cm}^{-1}$ , in both directions, although much sharper when light was polarized parallel to the  $a$ -axis. The irreducible vibrational representation of  $\text{TaNiTe}_5$  is:

$$\Gamma_{\text{irr}} = 10A_g + 10B_{1g} + 8B_{2g} + 8B_{3g} + 9B_{1u} + 10B_{2u} + 11B_{3u}.$$

The  $A_g$  and  $B_g$  modes are Raman active, while only the  $B_u$  modes are infrared active. A calculation using an empirical (normal coordinate analysis, or force field model)

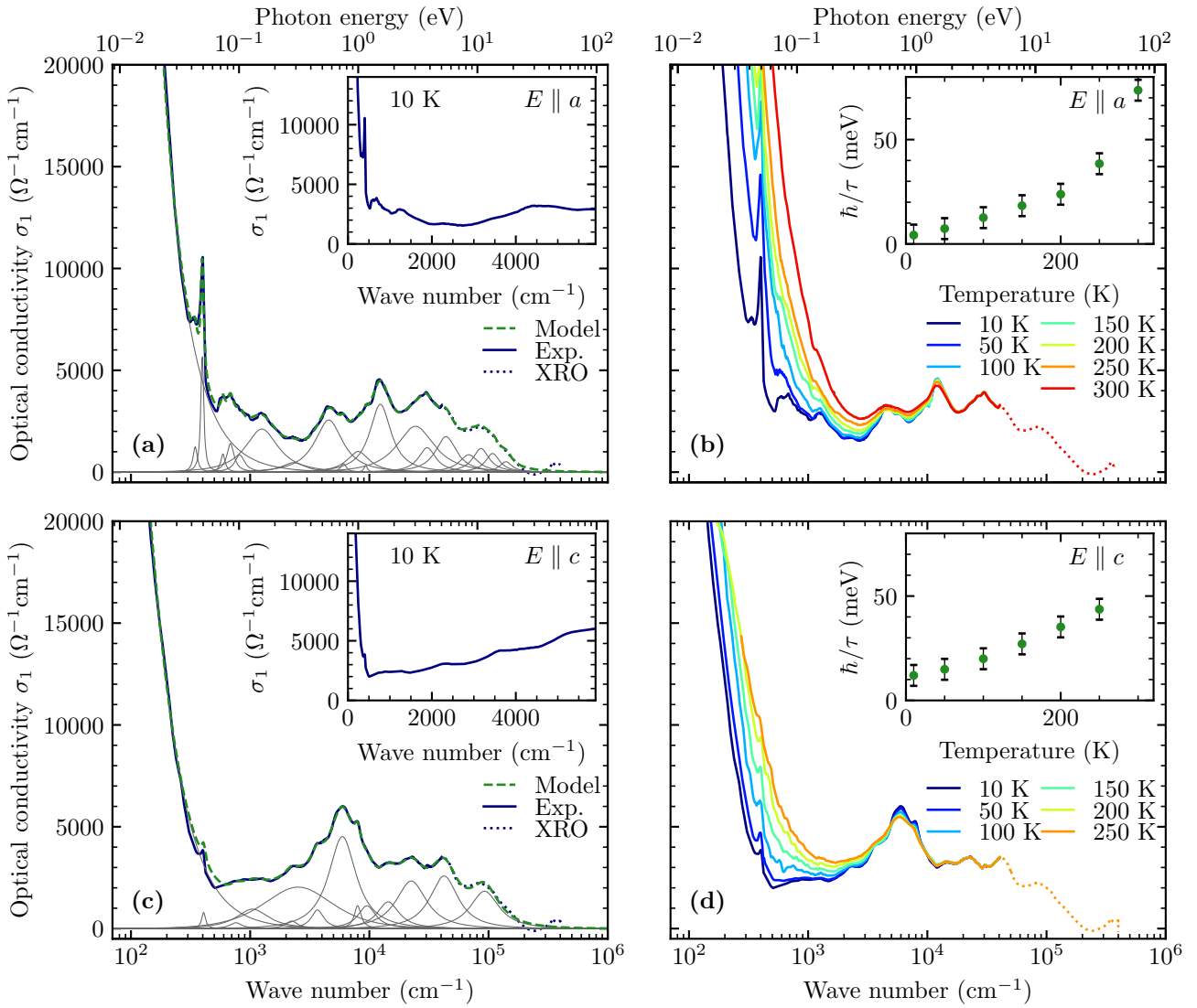


Figure 3. (a) The the real part of the optical conductivity ( $\sigma_1$ ) of TaNiTe<sub>5</sub> along the  $a$  axis at 10 K. The conductivity decomposition was obtained by fitting  $\sigma_1(\omega)$  to the Drude-Lorentz sum, Eq. (1). The Drude-Lorentz conductivity fit is shown by the dashed line. It contains a strong and narrow Drude response, characterized as Lorentzian centered as zero frequency with a full width at half maximum of  $1/\tau$ , a sharp and narrow lattice contribution (phonon line), and a number of bound excitations attributed to interband transitions. The dotted line shows data that was extrapolated from X-ray scattering functions (XRO) [11]. The inset shows the low-energy range of the optical conductivity with a linear scale. (b) The temperature dependence of the real part of optical conductivity along the  $a$  direction. The inset shows temperature dependence of scattering rate acquired from Drude-Lorentz fits. Dotted line shows data that was generated from XRO. This analysis has been repeated for the  $c$ -axis optical conductivity, shown in (c) and (d).

[17] gives one strong mode along the  $a$  axis, which we identify as a  $B_{3u}$  mode, at a frequency consistent with our measurements.

The optical response at energies above the Drude term contains multiple interband transitions which we fit by seven Lorentzian oscillators in the Drude-Lorentz model, shown in Figs. 3(a) and 3(c). There are no apparent traces of low dimensionality in  $\sigma_1(\omega)$  in  $a$  and  $c$  directions, contrary to what is expected for a quasi-1D mate-

rial [18]. A low-dimensional band dispersion leads to a flat band for certain  $k$ -space directions. This results in van Hove singularities [19]. In optical conductivity, such van Hove singularities would be visible as sharp peaks or sharp onsets of absorption.

Since TaNiTe<sub>5</sub> has been reported to be a nodal line semimetal, it makes sense to compare it with other such materials, for example the representative square net lattice systems ZrSiS [20], ZrSiSe [21] and BaNiS<sub>2</sub> [22]. In

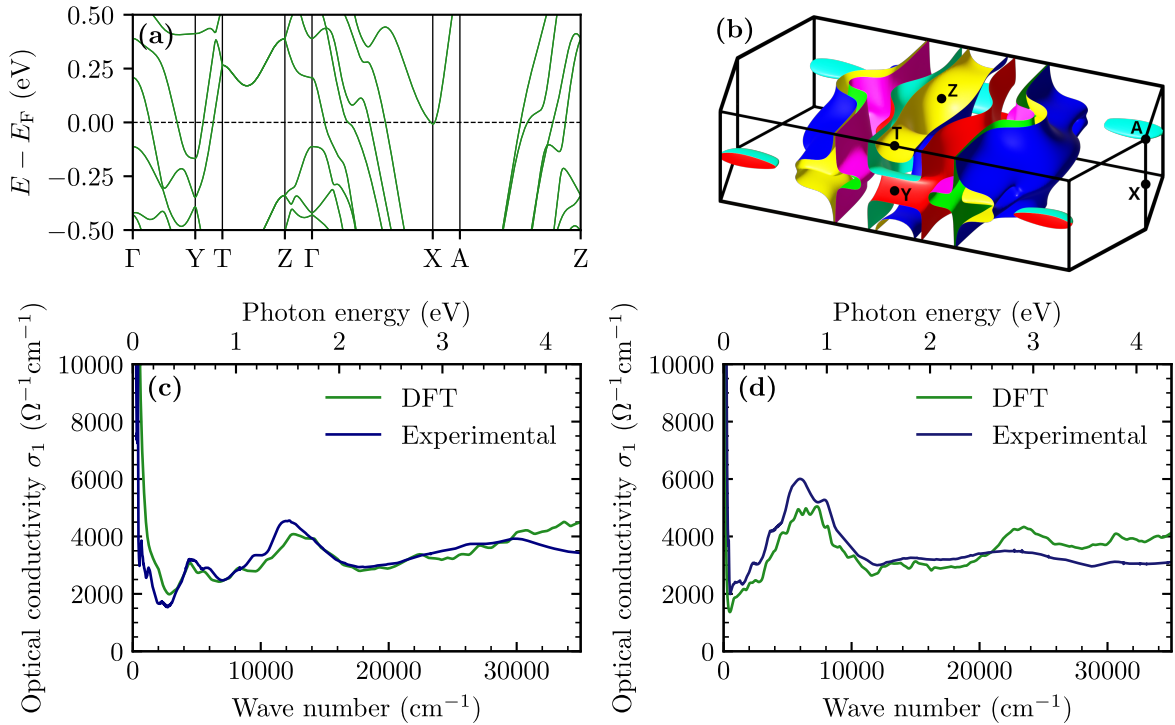


Figure 4. (a) Calculated band structure for  $\text{TaNiTe}_5$  along the high-symmetry directions. (b) Calculated Fermi surface, which contains strongly warped 2D sheets and 3D pockets. (c) Comparison between the DFT-calculated and experimental real parts of the optical conductivity along the  $a$  axis, and (d) along the  $c$  axis.

all of these nodal line semimetals, there is a fairly flat part in  $\sigma_1(\omega)$ , with little frequency dependence, and a temperature-induced spectral weight transfer. The spectral weight moves from energies above the region of flat  $\sigma_1(\omega)$  to energies below that region. No similar behavior can be seen in  $\text{TaNiTe}_5$ . Instead, a strong Drude contribution is followed by a series of broad, frequency-dependent excitations.

Figure 4(a) shows the calculated band structure along the high-symmetry directions, resulting in a composite Fermi surface shown in Fig. 4(b). As a result of structural features, the calculated Fermi surface consists of strongly warped 2D sheets, an interconnected tubular pocket with open orbits along both the  $c$  and  $b$  directions, and ellipsoidal 3D pockets. The 2D sheets reflect a structural motif of tantalum and nickel polymer chains running along the  $a$  direction. From this calculation, the optical conductivity, shown in Figs. 4(c) and 4(d) for the two light polarizations, can be determined. Since the band structure shows multiple bands crossing the Fermi level, we expect multiple Drude contributions in optical conductivity. Furthermore, multiple bands above and below the Fermi level allow for a number of interband transitions to be excited. Many of these bands are parallel, leading to an enhanced joint density of states. Each of the transitions can be seen as a feature in the optical conductivity, providing an explanation for multiple peaks in

the measured data. In general, the *ab initio* calculations correspond very well to the experimental optical conductivity.

#### IV. CONCLUSION

We have measured the temperature dependence of the electronic transport and determined the complex optical properties of  $\text{TaNiTe}_5$  along the  $a$  and  $c$  crystallographic axes. The optical conductivity shows metallic-like behavior in both directions. Resistivity measurements show noticeable anisotropy and linear temperature dependence above 100 K consistent with electron-phonon scattering. Using Kramers-Kronig transformations, we calculated optical response functions and analyzed them using the Drude-Lorentz model. *Ab initio* calculations agree very well with the optical conductivity data. This gives confidence that the calculated band structure of  $\text{TaNiTe}_5$  correctly describes this material. Infrared spectroscopy shows that  $\text{TaNiTe}_5$  is an anisotropic semimetal with low scattering rates and pronounced interband transitions. Neither in the calculation nor in the infrared measurements can one see any clear signatures of reduced dimensionality.

## V. ACKNOWLEDGMENTS

This research was supported by the NCCR MARVEL, a National Centre of Competence in Research, funded by the Swiss National Science Foundation (Grant No. 205602). A.A. acknowledges funding from the Swiss National Science Foundation through Project No. PP00P2\_202661. Work at Brookhaven National Laboratory was supported by the Office of Science, U.S. Department of Energy, under Contract No. DE-SC0012704. N.B., A.A. and J.B. acknowledge the support of the Croatian Science Foundation under Project No. IP-2022-10-

3382. M.N. and N.B. acknowledge the support of the CeNIKS project co-financed by the Croatian Government and the EU through the European Regional Development Fund Competitiveness and Cohesion Operational Program (Grant No. KK.01.1.1.02.0013). A.A. and M.N. acknowledge funding from the Swiss National Science Foundation, through the instrument Scientific Exchanges, Grant number 199151. J.M. and A.P. were supported by the project Quantum materials for applications in sustainable technologies (QM4ST), funded as project No. CZ.02.01.01/00/22.008/0004572 by P JAK, call Excellent Research. The work at the TU Wien was supported by FWF Project P 35945-N.

---

[1] S. Siddique, C. C. Gowda, S. Demiss, R. Tromer, S. Paul, K. Kumar, K. K. Sadasivuni, E. F. Olu, A. Chandra, V. Kochat, D. S. G. ao, P. Kumbhakar, R. Mishra, P. M. Ajayan, and C. S. Tiwary, Emerging two-dimensional tellurides, *Materials Today* **51**, 402 (2021).

[2] H. R. Banjade, J. Pan, and Q. Yan, Monolayer 2d semiconducting tellurides for high-mobility electronics, *Phys. Rev. Mater.* **5**, 014005 (2021).

[3] C. Xu, Y. Liu, P. Cai, B. Li, W. Jiao, Y. Li, J. Zhang, W. Zhou, B. Qian, X. Jiang, Z. Shi, R. Sankar, J. Zhang, F. Yang, Z. Zhu, P. Biswas, D. Qian, X. Ke, and X. Xu, Anisotropic Transport and Quantum Oscillations in the Quasi-One-Dimensional TaNiTe<sub>5</sub>: Evidence for the Non-trivial Band Topology, *J. Phys. Chem. Lett.* **11**, 7782 (2020).

[4] Y. Huang, R. Ye, W. Shen, X. Yao, and G. Cao, Magnetic Field-Induced Resistivity Upturn and Non-Topological Origin in the Quasi-One-Dimensional Semimetals, *Symmetry* **15**, 1882 (2023).

[5] Z. Hao, W. Chen, Y. Wang, J. Li, X.-M. Ma, Y.-J. Hao, R. Lu, Z. Shen, Z. Jiang, W. Liu, Q. Jiang, Y. Yang, X. Lei, L. Wang, Y. Fu, L. Zhou, L. Huang, Z. Liu, M. Ye, D. Shen, J. Mei, H. He, C. Liu, K. Deng, C. Liu, Q. Liu, and C. Chen, Multiple Dirac nodal lines in an in-plane anisotropic semimetal TaNiTe<sub>5</sub>, *Phys. Rev. B* **104**, 115158 (2021).

[6] Y. Li, Z. Ran, C. Huang, G. Wang, P. Shen, H. Huang, C. Xu, Y. Liu, W. Jiao, W. Jiang, J. Hu, G. Zhu, C. Xu, Q. Lu, G. Wang, Q. Jing, S. Wang, Z. Shi, J. Jia, X. Xu, W. Zhang, W. Luo, and D. Qian, Coexistence of Ferroelectriclike Polarization and Dirac-like Surface State in TaNiTe<sub>5</sub>, *Phys. Rev. Lett.* **128**, 106802 (2022).

[7] R. Ye, T. Gao, H. Li, X. Liang, and G. Cao, Anisotropic giant magnetoresistance and de Hass–van Alphen oscillations in layered topological semimetal crystals, *AIP Advances* **12**, 045104 (2022).

[8] Z. Chen, M. Wu, Y. Zhang, J. Zhang, Y. Nie, Y. Qin, Y. Han, C. Xi, S. Ma, X. Kan, J. Zhou, X. Yang, X. Zhu, W. Ning, and M. Tian, Three-dimensional topological semimetal phase in layered TaNiTe<sub>5</sub> probed by quantum oscillations, *Phys. Rev. B* **103**, 035105 (2021).

[9] N. Ma, D.-Y. Wang, B.-R. Huang, K.-Y. Li, J.-P. Song, J.-Z. Liu, H.-P. Mei, M. Ye, and A. Li, Quasi-one-dimensional characters in topological semimetal TaNiTe<sub>5</sub>, *Chinese Physics B* **32**, 056801 (2023).

[10] C. C. Homes, M. Reedyk, D. A. Crandles, and T. Timusk, Technique for measuring the reflectance of irregular, submillimeter-sized samples, *Appl. Opt.* **32**, 2976 (1993).

[11] D. B. Tanner, Use of x-ray scattering functions in Kramers-Kronig analysis of reflectance, *Phys. Rev. B* **91**, 035123 (2015).

[12] A. B. Kuzmenko, Kramers–Kronig constrained variational analysis of optical spectra, *Review of Scientific Instruments* **76**, 083108 (2005).

[13] The Elk Code, <http://elk.sourceforge.net/>.

[14] J. P. Perdew, K. Burke, and M. Ernzerhof, Generalized Gradient Approximation Made Simple, *Phys. Rev. Lett.* **77**, 3865 (1996).

[15] E. W. Liimatta and J. A. Ibers, Synthesis, structures, and conductivities of the new layered compounds Ta<sub>3</sub>Pd<sub>3</sub>Te<sub>14</sub> and TaNiTe<sub>5</sub>, *Journal of Solid State Chemistry* **78**, 7 (1989).

[16] K. Momma and F. Izumi, VESTA 3 for three-dimensional visualization of crystal, volumetric and morphology data, *J. Appl. Crystr.* **44**, 1272 (2011).

[17] E. Dowty, computer code, VIBRATZ (Shape Software, Kingsport, TN, 2001).

[18] C. C. Homes, Q. Du, C. Petrovic, W. H. Brito, S. Choi, and G. Kotliar, Unusual electronic and vibrational properties in the colossal thermopower material FeSb<sub>2</sub>, *Scientific Reports* **8**, 11692 (2018).

[19] P. Y. Yu and M. Cardona, *Fundamentals of Semiconductors* (Springer, Berlin Heidelberg, 2010).

[20] M. B. Schilling, L. M. Schoop, B. V. Lotsch, M. Dressel, and A. V. Pronin, Flat Optical Conductivity in ZrSiS due to Two-Dimensional Dirac Bands, *Phys. Rev. Lett.* **119**, 187401 (2017).

[21] Y. Shao, A. N. Rudenko, J. Hu, Z. Sun, Y. Zhu, S. Moon, A. J. Millis, S. Yuan, A. I. Lichtenstein, D. Smirnov, Z. Q. Mao, M. I. Katsnelson, and D. N. Basov, Electronic correlations in nodal-line semimetals, *Nature Physics* **16**, 636 (2020).

[22] D. Santos-Cottin, M. Casula, L. de’ Medici, F. Le Mardelé, J. Wyzula, M. Orlita, Y. Klein, A. Gauzzi, A. Akrap, and R. P. S. M. Lobo, Optical conductivity signatures of open Dirac nodal lines, *Phys. Rev. B* **104**, L201115 (2021).